

Fracture surface roughness in highly deformable polymers

Y. FUKAHORI*, E. H. ANDREWS

Department of Materials, Queen Mary College, London, UK

The fracture surface roughness was determined for five highly deformable polymers (styrene-butadiene rubber, two ethylene-propylene rubbers, low density polyethylene and plasticized polyvinyl chloride) as a function of rate and temperature. The mechanical hysteresis for the same materials was also measured as a function of rate, temperature and strain amplitude. Although the surface roughness does not correlate with crack velocity, it does so uniquely with the effective hysteresis in the material surrounding the propagating crack. A simple physical explanation is advanced for the universal dependence of roughness on hysteresis in these materials.

1. Introduction

The study of fracture surfaces ("fractography") reveals a great deal of information about the fracture process including the point of crack nucleation, the direction and velocity of crack propagation and the incidence of secondary fracture. On a more subtle level, the nature of the fracture surface reflects the mechanical processes of deformation and energy supply which maintain or increase the velocity of fracture propagation. Fractography may therefore supplement a study of the mechanics of fracture such as is reported elsewhere [1, 2] for the materials considered in the paper.

The fracture surfaces of polymers have been discussed by many authors and reviewed by Wolock and Newman [3] and by Andrews [4]. In particular, the surface roughness in rigid polymers tends to increase with increasing specimen strain rate and crack velocity and to decrease with increasing temperature [5-7]. In elastomeric polymers, Thomas and Greensmith [8] reported rough or irregular surfaces in natural rubber and styrene-butadiene rubber at low rates of crack growth, with a transition to smoother appearances as higher velocities. For SBR a critical transition

velocity of around 10^{-4} m sec⁻¹ was identified [9] at room temperature, but at 90°C surfaces were smoother and insensitive to crack speed [10]. Carbon filled SBR had much smoother fracture surfaces than the unfilled rubber. Other workers have found similar results [11, 12] though Mason suggested a smooth → rough → smooth progression with increasing crack velocity in NR and SBR.

There is general agreement, however, that in elastomers increased crack speed gives smoother surfaces whereas in rigid polymers the reverse is generally true. One possible reason for this is that the two types of polymer fall on different sides of the glass transition temperature, so that their mechanical loss (hysteresis) is affected differently by changes in deformation rates and thus crack velocity.

A recent study of the mechanics of crack propagation in highly deformable and inelastic polymers, focuses attention on the role of mechanical hysteresis in fracture [2]. It is the purpose of this paper to show that surface roughness in these types of polymer also correlates strongly with hysteresis and to advance a possible explanation.

*On leave of absence from the Bridgestone Tyre Company, Research Department, 2800-Ogawa Higashi-Machi, Kodairy-shi, Tokyo, Japan.

2. Experimental

2.1. Materials

The materials studied were three cross-linked elastomers (styrene butadiene rubber, SBR; ethylene propylene diene rubber, EPDM of molecular mass 100 000; and EPDM(s) of molecular mass 43 000), and two highly deformable thermoplastics (low density polyethylene, PE, and plasticized polyvinyl chloride, p-PVC). The relevant compounding details for the elastomers are given in [2].

Test specimens were cut from compression moulded sheets approximately 1 mm thick and took the form of dumb-bell specimens with a gauge length measuring 2 cm × 0.6 cm and parallel-sided specimens 5 cm × 1 cm or 2 cm × 0.6 cm containing an edge crack of ~1 mm positioned centrally to the length of the strip. The edge cracks were formed with a razor blade.

2.2. Crack velocity measurements

These measurements were made on the edge-crack specimens. Each specimen was extended at a selected constant cross-head speed (and thus a constant strain rate) for a time t_1 and returned to zero strain rapidly in time t_2 ($t_2 \sim 10^{-2} t_1$). The crack growth Δc was measured in the unstrained state and the growth in time t_2 was neglected as being very small. A plot of Δc versus t_1 was thus produced and the slope at any time t_1 taken as the instantaneous velocity. The same data also provide crack velocity as a function of crack length c . The measurements were repeated at different cross-head speeds and at temperatures in the range 24 to 100°C. Dumb-bell specimens were also tested to failure under the same conditions for later comparison of fracture surfaces.

2.3. Hysteresis measurements

Load-deflection cycles were recorded on un-notched dumb-bell specimens at different strain rates and temperatures and the hysteresis ratio obtained as a function of strain, strain rate and temperature from;

$$h = (W_0 - W_R)/W_0$$

where W_0 is the input energy density of deformation up to the point of strain reversal and W_R is the retraction energy density (given by the area under the retraction stress-strain curve).

2.4. Measurement of surface roughness

The fracture surfaces of specimens produced by the procedure described in Section 2.2 were examined by optical photomicroscopy. To improve visibility of surface features the surfaces were first metallized by a light evaporated Al coating.

Although variations in surface roughness are obvious to the eye it is less easy to quantify the roughness, especially as the scale of roughness is too gross in these materials for effective use of instruments such as the "Talysurf". A simple but effective measure of roughness was therefore obtained by the following procedure.

Photographic prints of the fracture surfaces were made and lines were drawn at $\pm 45^\circ$ to the direction of propagation. The number of intersections (per unit length of these lines) with ridges on the fracture surface was counted, but each ridge was also weighted on an arbitrary four-point scale (0.5, 1, 2, 3) according to its apparent thickness or intensity on the print. This takes account of variations in the height of steps or ridges as well as their frequency. The resulting number we call the "roughness index" or RI.

3. Results

3.1. Crack velocity

Crack velocity data is given as a function of crack growth X in Fig. 1 for all materials (except PE) at 24°C. In this diagram, crack velocity has been divided by cross-head speed, the latter quantity varying by a factor of forty from 8.33×10^{-6} to 3.33×10^{-4} m sec⁻¹. The effect of this normalization is to give an almost unique curve for each material showing that crack velocity is nearly proportional to the cross-head speed (at a given crack length) for these highly extensible materials, tending towards a situation where crack velocity roughly equals the grip separation speed. This dependence on cross-head speed is, of course, additional to the effect of energy release rate which increases the crack velocity by factors of 10^2 to 10^3 under the influence of the increasing strain and crack length. That crack velocity is not controlled *solely* by energy release rate is almost certainly due to the large mechanical hysteresis in these materials.

The crack velocity, of course, determines the straining rate in the highly strained zone surrounding the crack tip, whereas the cross-head

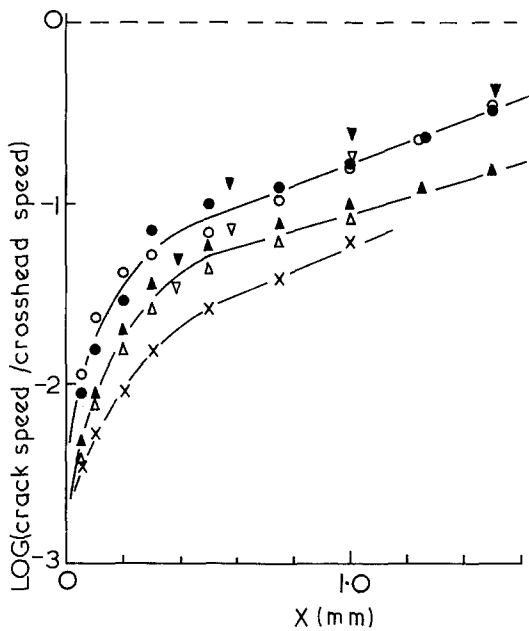


Figure 1 Ratio of crack speed to cross-head speed as a function of crack extension X for four different materials. (○) SBR (△) EPDM (X) EPDM (s) and (△) p-PVC. Open symbols at cross-head speed of $3.33 \times 10^{-4} \text{ m sec}^{-1}$, filled symbols at $8.33 \times 10^{-6} \text{ m sec}^{-1}$. For each material crack speed is nearly proportional to cross-head speed at a given crack length.

speed determines the straining rate in the bulk of the specimen. In particular, we can write the local strain rate near the crack tip as

$$\dot{\epsilon}_L = \frac{d\epsilon_L}{dX} \frac{dX}{dt} = \frac{-d\epsilon_L}{dX} c \quad (1)$$

where X is distance measured along the crack axis. The strain gradient $-d\epsilon_L/dX$ is a positive quantity

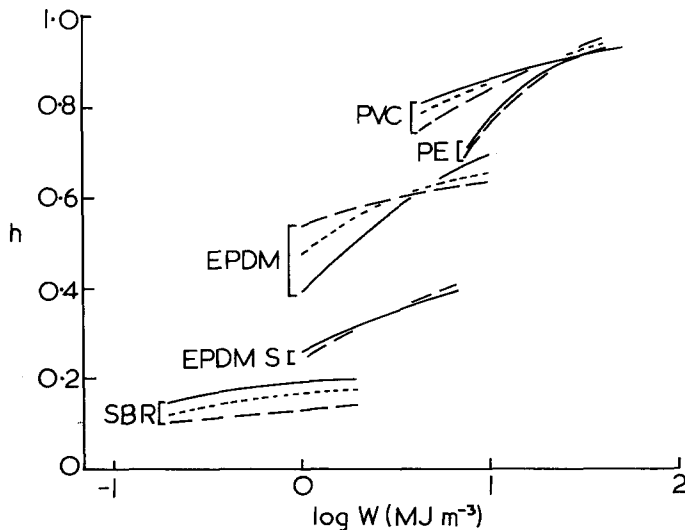


Figure 2 Hysteresis ratio h as a function of input energy density W for five materials. Solid lines at strain rate of $1.67 \times 10^{-2} \text{ s}^{-1}$, dotted lines at $6.67 \times 10^{-4} \text{ sec}^{-1}$ and broken lines at $1.67 \times 10^{-5} \text{ sec}^{-1}$.

(in the loading zone) which varies from point to point in the stress field. Values for this quantity were obtained for some of the materials used in this study in the course of another investigation [2] and vary from zero to $5 \times 10^3 \text{ m}^{-1}$.

The highest crack velocities encountered in this study were of the order of $10^{-4} \text{ m sec}^{-1}$ so that the global variation in strain rates is from about 10^{-4} sec^{-1} for the bulk of slowly extended specimens to $5 \times 10^{-1} \text{ sec}^{-1}$ for some local regions close to the propagating crack. These figures are important when attempts are made later to assign an effective hysteresis ratio to the material in the vicinity of the propagating crack.

3.2. Hysteresis ratio

The collected room temperature data for h as a function of input energy density W_0 , is presented in Fig. 2, experimental points being omitted for clarity (there is no significant scatter). For each material data are presented at three strain rates from 1.67×10^{-5} to $1.67 \times 10^{-2} \text{ sec}^{-1}$. The highest strain rate is some 30 times smaller than the highest strain rate expected in the vicinity of a crack tip (see previous section), but this maximum strain rate applies over only a very small volume of the highly strained zone at the tip. Furthermore, except for EPDM, the effects of strain rate on h are not great and can be extrapolated with some confidence to higher rates.

The range of strain (or W) values covered by the data is from about 0.1 to 0.9 of the strain (or energy density) to failure in tension and thus covers the states of strain encountered throughout almost the entire specimen including the crack tip

zone. Although, therefore, the hysteresis data do not *completely* cover the ranges of strain and strain rate experienced by the material around a propagating crack, they do so for most regions of the specimen.

In order to assign an effective or average value (\bar{h}) of h to any crack propagation event we proceed as follows. To allow for point-to-point *strain* variations in the crack tip zone, we take the average value of h obtained at different strains (at a given strain rate, for a given material) from the uniaxial data. In taking this average, the minimum strain admitted is of course the bulk strain of the crack propagation specimen. Since the arithmetical average is unlikely to be the "effective" value of h (which in any case is difficult to define), error bars are included for each point showing the maximum and minimum values of h obtained, with respect to strain, from the uniaxial data.

To allow for *strain rate* variations in \bar{h} , we note that the local strain rate is proportional to crack velocity which in turn is proportional (at a given crack length) to the grip separation speed or overall specimen strain rate. Similarly, the strain rate at points remote from the crack will be

proportional to the overall strain rate. Thus the specimen strain rate can be used as a scaling factor for strain rates throughout the specimen.

Of course, as we have already seen, *local* strain rates vary from the overall specimen value up to $5 \times 10^{-1} \text{ sec}^{-1}$ whereas our hysteresis data was obtained only up to strain rates of about $1.7 \times 10^{-2} \text{ sec}^{-1}$. However, Fig. 2 shows that the effect on h of strain rate, over three decades, is either very small or else reverses sign over the range of energy densities (or strain levels) present around the crack tip. To a first approximation, therefore, relatively small errors should be introduced by adopting the overall specimen strain rate as the effective strain rate for the assignation of an effective hysteresis \bar{h} to a given fracture surface. Finally, the variation of \bar{h} , and its error bars, with temperature for the four materials at a given strain rate is shown in Fig. 3 and reveals the anticipated decrease with rising temperature typical of elastomeric materials.

It is now possible to assign a value of \bar{h} (including error bars) to each fracture surface produced in a given material at a given specimen strain rate (or crack velocity) and temperature.

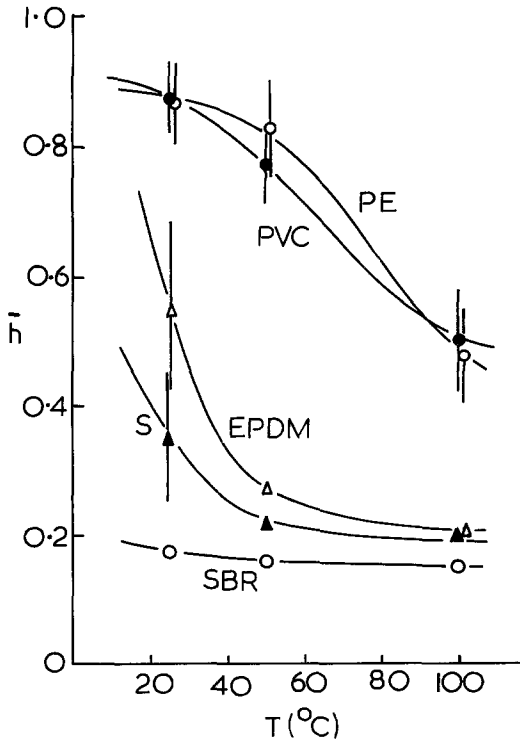


Figure 3 Hysteresis ratio \bar{h} as a function of temperature for five materials. Curve marked S is for EPDM(s). Bars show spread of h with energy density and strain rate.

3.3. Surface roughness and hysteresis ratio

Examples of the surfaces obtained are given in Fig. 4a for SBR and Fig. 4b for p-PVC. It is visually apparent that surface roughness varies with length along the specimen (thus with \dot{c}), with temperature and with specimen strain rate (also affecting \dot{c}). When analysed, however, it becomes clear that the dependence of RI on crack velocity is ambiguous. Fig. 5 shows RI plotted logarithmically against crack velocity for the three elastomers. For SBR the roughness decreases with \dot{c} but for EPDM it increases and for EPDM(s) it is insensitive to changes in velocity over four decades.

A universal correlation between roughness and crack velocity is thus impossible. However, new light emerges on this problem when the behaviour of the hysteresis ratio is examined. Fig. 6 shows \bar{h} plotted against the cross-head speed at which it was measured, for the same three materials. We see that for SBR, \bar{h} increases with strain rate, for EPDM it decreases and for EPDM(s), \bar{h} is insensitive to rate. Taking the data of Figs. 5 and 6 together we see emerging a qualitative correlation between RI and \bar{h} , i.e. when \bar{h} is large, the RI is small and vice versa.

This correlation is confirmed by plotting,

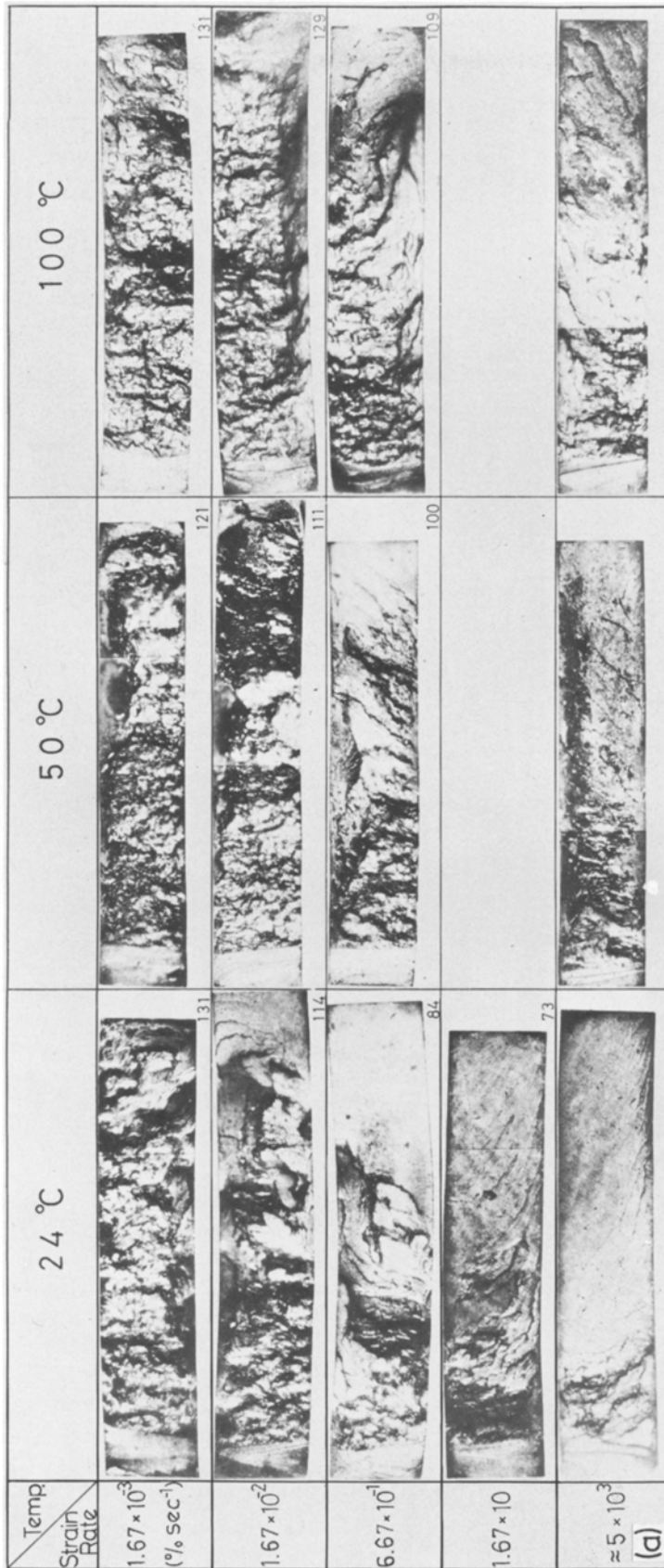


Figure 4 (a) Fracture surfaces of SBR under the conditions shown. Figures in right hand corners are the roughness indices.














Temp.	Strain Rate (% sec ⁻¹)		
100 °C	4.17×10^3		41
	4.17×10^2		46
	1.67		44
	$\approx 5 \times 10^3$		
50 °C	4.17×10^3		28
	4.17×10^2		29
	1.67		30
	$\approx 5 \times 10^3$		
24 °C	4.17×10^3		23
	4.17×10^2		19
	1.67		26
	4.17×10		29
	$\approx 5 \times 10^3$		
(b)			

Figure 4 (b) Fracture surfaces of p-PVC.

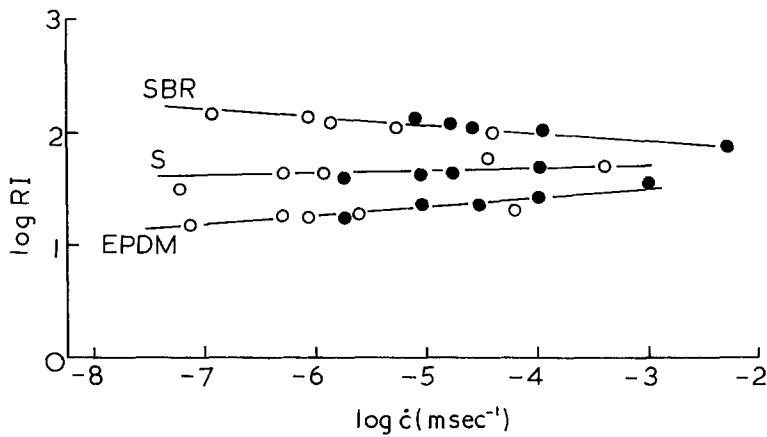


Figure 5 Dependence of roughness index (RI) upon crack velocity for three materials. S denotes EPDM (s). Open symbols at cross-head speed of 8.33×10^{-6} m sec^{-1} , filled symbols at 3.33×10^{-4} m sec^{-1} .

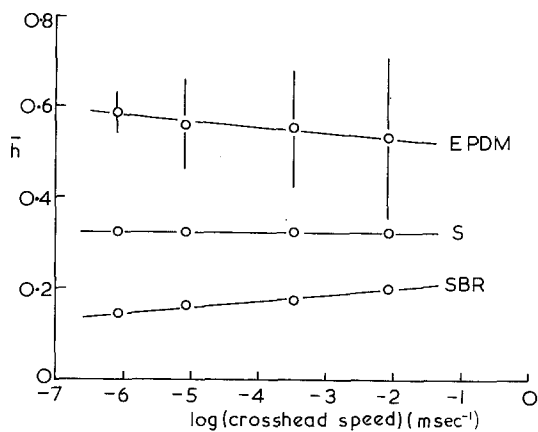


Figure 6 Dependence of hysteresis ratio \bar{h} on cross-head speed at which it is measured. S denotes EPDM (s). Bars indicate spread of \bar{h} with respect to input energy density.

logarithmically, hysteresis ratio \bar{h} against RI (averaged over a given surface to eliminate crack length dependence), as shown in Fig. 7. This plot includes all data for different crack velocities, temperatures and materials. The slope of the line is such that

$$\bar{RI} = \text{constant} \times \bar{h}^{-1} \quad (2)$$

To illustrate the effect of crack length, RI was also measured at different points along selected surfaces and an \bar{h} value assigned by taking the effective strain rate as

$$\dot{\epsilon}_{\text{eff}} = (\dot{c}/\dot{c}_f)\dot{\epsilon}_0 \quad (3)$$

where \dot{c} is the crack velocity at the measured point, \dot{c}_f the final crack velocity and $\dot{\epsilon}_0$ the previously employed overall specimen strain rate.

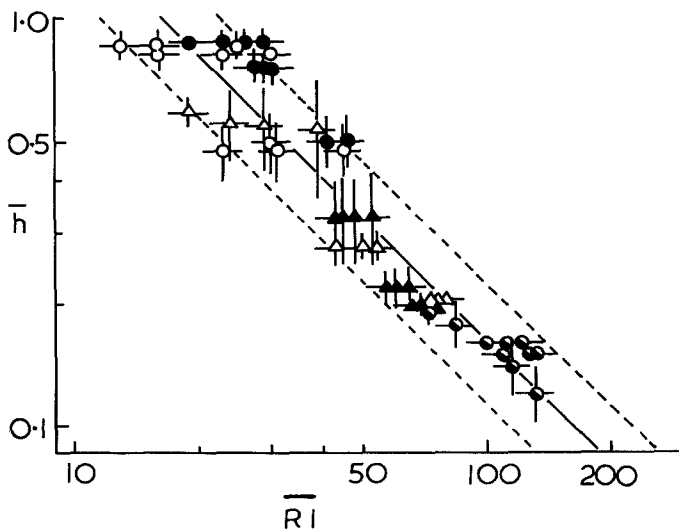


Figure 7 Correlation between hysteresis ratio \bar{h} averaged over each fracture surface, and the mean roughness index for that surface. Five materials and various temperatures. (○) PE (●) p-PVC (△) EPDM (▲) EPDM (◐) SBR.

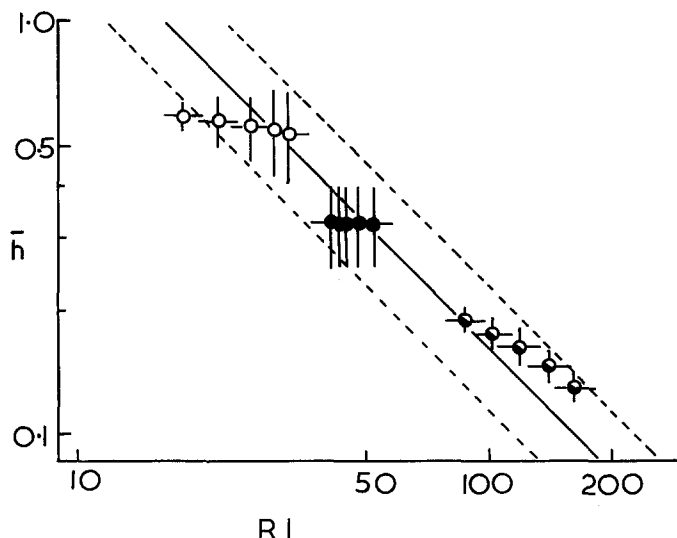


Figure 8 Correlation between hysteresis ratio \bar{h} at a point on a fracture surface (thus at a given fracture velocity) and the roughness index at that point. All test at 24° C (○) EPDM (●) EPDM (s) and (s) SBR. Correlation band taken from Fig. 7.

These values, RI (not averaged), are plotted logarithmically against \bar{h} in Fig. 8 and are seen to fall within the scatter band defined by Fig. 7 and which is included in Fig. 8. It appears therefore that hysteresis is the major factor determining fracture surface roughness in elastomeric materials.

4. Discussion

A fairly simple explanation can be advanced to explain the inverse correlation between surface roughness and mechanical hysteresis. This explanation has the added merit of reconciling the observations on fracture surfaces in brittle solids and highly deformable ones.

The basic idea adopted here is that surface roughness arises from secondary fracture i.e. fracture initiated ahead, and to either side, of the primary fracture. Secondary fractures occur when the high stresses surrounding the primary fracture front encounter microscopic stress-raisers or regions of weakness in the path of the crack [4]. If a secondary fracture grows significantly before it is overtaken by the primary front it may join up with the primary fracture, even though it lies in a different plane, by shear of the intervening material (See Fig. 9). Surface roughness is thereby generated. This explanation was given for surface roughness in brittle solids as long ago as 1936 by Smekal [13].

Consider now a visco-elastic solid. The propagation of fracture in such a material is describable by Andrews' equation [14],

$$\mathcal{F} = \mathcal{F}_0 \Phi(\dot{c}, T, \epsilon_0) \quad (4)$$

where \mathcal{F} is the fracture surface energy, \mathcal{F}_0 the true surface energy and Φ a loss function which for our present purpose can be written in the form

$$\Phi = \{1 - f(\bar{h})\}^{-1} \quad (5)$$

where f is a function. Thus as \bar{h} increases Φ also increases, as does \mathcal{F} . Further, for short cracks,

$$\mathcal{F} = k_1 c W \quad (6)$$

where k_1 is a slowly varying term, c the crack length and W the strain energy density.

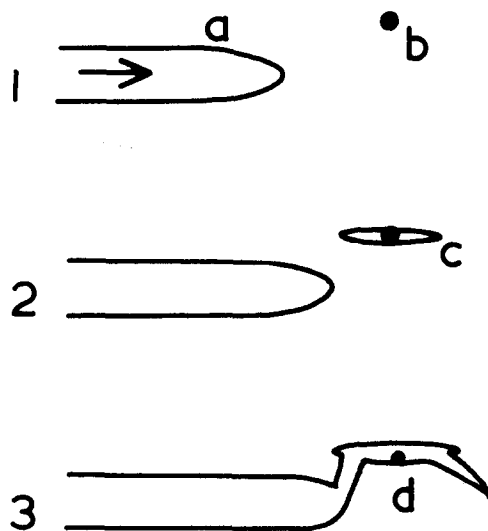


Figure 9 Formation of roughness by secondary fracture (schematic); (a) crack, (b) stress-raiser, (c) secondary crack, (d) roughness step caused by diversion of primary crack.

Applying this to the growth of a secondary fracture it will be seen that the strain (or energy density) required to propagate the fracture increases with the hysteresis ratio \bar{h} of the material.

Alternatively, in a given strain field surrounding the primary fracture, secondary fractures will occur in a *smaller zone* surrounding the primary crack if \bar{h} is larger (since strain level decays with distance from the primary crack tip). Since the scale of roughness will relate directly to the separation of the planes of primary and secondary fracture, this means that high hysteresis will produce a lower degree of roughness.

This can be expressed mathematically. Consider a secondary crack [c_2] of length c_2 in the strain field of a primary crack [c_1] of length c_1 . Let r be the radial distance of c_2 from the tip of c_1 , W_0 the applied energy density remote from [c_1] and W the energy density at a point in the stress field around [c_1]. The decay of W with r is known [15] to be of the form

$$W = \frac{\alpha W_0 c_1}{r} \quad (7)$$

where α is a constant. If W_{crit} is the critical energy density needed to cause [c_2] to propagate, then

$$\mathcal{G} = k_1 c_2 W_{\text{crit}} \quad (8)$$

and [c_2] will only grow if it lies within a distance $r = R$ of the primary crack, where

$$R = \frac{\alpha W_0 c_1}{W_{\text{crit}}} = \frac{W_0 c_1 k_1 c_2}{\mathcal{G}} \quad (9)$$

From Equation 4, then,

$$R = W_0 c_1 c_2 k_1 \{1 - f(\bar{h})\} / \mathcal{G}_0 \quad (10)$$

and R will be the scale of roughness in the surface i.e. the maximum vertical displacement of the fracture surface.

Although R will not be the same as the roughness index previously defined, it will be related to it. Equation 10 shows R increasing with the overall applied energy density (thus with the applied stress or strain), with crack length c_1 , with secondary flaw size c_2 and with decreasing hysteresis ratio \bar{h} . These predictions are all in accord with observation.

References

1. Y. FUKAHORI, Ph.D. thesis, University of London, 1976.
2. E. H. ANDREWS and Y. FUKAHORI, *J. Mater. Sci.* **12** (1977) 1307.
3. S. B. NEWMAN and I. WOLOCK, *J. Res. Natl. Bur. Stand.* **58** (1957) 339.
4. E. H. ANDREWS, "Fracture in Polymers" (Oliver & Boyd, London, 1968) p. 177.
5. L. J. BROUTMAN and F. J. MCGARRY, *J. Appl. Polym. Sci.* **9** (1965) 589.
6. A. T. DIBENEDETTO and K. L. TRACHTE, *ibid* **14** (1970) 2249.
7. A. G. ATKINS, C. S. LEE and R. M. CADDELL, *J. Mater. Sci.* **10** (1975) 1381.
8. A. G. THOMAS and H. W. GREENSMITH, *J. Polym. Sci.* **18** (1955) 189.
9. A. G. THOMAS, *J. Appl. Polym. Sci.* **3** (1960) 168.
10. H. W. GREENSMITH, *ibid* **3** (1960) 183.
11. P. MASON, *ibid* **29** (1958) 1146.
12. W. G. KNAUSS, Proceeding of the International Conference of Fracture, 2 Sendai, Japan, edited by T. Yokobori (1965) 1139.
13. A. SMEKAL, *Ergeb. Exakt. Naturw.* **15** (1936) 106.
14. E. H. ANDREWS, *J. Mater. Sci.* **9** (1974) 887.
15. *Idem*, *Proc. Phys. Soc. (London)* **77** (1961) 483.

Received 17 May and accepted 29 July 1977.